Journal of Magnetism and Magnetic Materials 401 (2016) 880–889

Contents lists available at ScienceDirect

Journal of Magnetism and Magnetic Materials

journal homepage: www.elsevier.com/locate/jmmm

Identification of ε-Fe_2O_3 nano-phase in borate glasses doped with Fe and Gd

O.S. Ivanova [a], R.D. Ivantsov [a], I.S. Edelman [a,*], E.A. Petrakovskaja [a], D.A. Velikanov [a,b], Y.V. Zubavichus [c], V.I. Zaikovskii [d,e], S.A. Stepanov [f]

[a] L.V. Kirensky Institute of Physics, Siberian Branch of RAS, 660036 Krasnoyarsk, Russia
[b] Siberian Federal University, 660036 Krasnoyarsk, Russia
[c] NRC "Kurchatov Institute", 123182 Moscow, Russia
[d] Boreskov Institute of Catalysis, Siberian Branch of RAS, 630090 Novosibirsk, Russia
[e] Novosibirsk State University, 630090 Novosibirsk, Russia
[f] Vavilov State Optical Institute, All-Russia Research Center, 192371 Petersburg, Russia

ARTICLE INFO

Article history:
Received 14 July 2015
Received in revised form
23 October 2015
Accepted 28 October 2015
Available online 31 October 2015

Keywords:
Magnetic nanoparticles
Epsilon-Fe_2O_3
Magnetic circular dichroism
Electron magnetic resonance

ABSTRACT

A new type of magnetic nanoparticles was revealed in borate glasses co-doped with low contents of iron and gadolinium. Structure and magnetic properties of the particles differ essentially from that of the α-Fe_2O_3, γ-Fe_2O_3, or Fe_3O_4 nanoparticles which were detected earlier in similar glass matrices. Transmission electron microscopy including STEM-HAADF and EDX, synchrotron radiation-based XRD, static magnetic measurements, magnetic circular dichroism, and electron magnetic resonance studies allow referring the nanoparticles to the iron oxide phase-ε-Fe_2O_3. Analysis of the data set has shown that it is Gd atoms that govern the process of nanoparticles' nucleation and its incorporation into the particles in different proportions can be used to adjust their magnetic and magneto-optical characteristics.

1. Introduction

Iron oxides traditionally take one of the central places in magnetic phenomena both from perspectives of fundamental investigations and industrial application. Up to latest years, investigators focused their efforts on three main types of iron oxide: magnetite Fe_3O_4, hematite α-Fe_2O_3, and maghemite γ-Fe_2O_3. Another iron (III) oxide polymorph, ε-Fe_2O_3, was probably synthesized for the first time by Forestier and Guiot-Guillain in 1934 who reported [1] a synthesis of ferric oxide with structure and properties distinctly different from those of γ-Fe_2O_3 and α-Fe_2O_3. The authors of Ref. [1] did not use the name ε-Fe_2O_3 for the synthesized compound. Later several authors reported on materials with the same properties, usually, mixed with γ-Fe_2O_3 and α-Fe_2O_3 [2–5]. R. Schrader and G. Buttner named the compound ε-Fe_2O_3 and determined its structure to be of monoclinic syngony with parameters $a=12.97$ Å, $b=10.21$ Å, $c=8.44$ Å, and $\beta=95.66°$ [2,6]. Dezsi and Coey [5] obtained a simpler crystal structure compared to that observed in [2,6]; nevertheless, they also refer it to ε-Fe_2O_3 subjected to disorder effects. E. Tronc, C. Chaneac, and J. P. Jolivet [7] have studied an influence of technological conditions on the ε-Fe_2O_3 phase structure and properties. They have shown that a high temperature heat treatment of γ-Fe_2O_3 nanoparticles dispersed in a silica xerogel gives rise to the formation of ε-Fe_2O_3 nanoparticles with a low content of α-Fe_2O_3 admixture phase. At that, ε-Fe_2O_3 nanoparticles of an average diameter of ~30 nm were described by the orthorhombic structure with $a=5.095$, $b=8.789$, and $c=9.437$ Å. This phase was shown to be isomorphs with $GaFeO_3$ [8], $AlFeO_3$ [9], κ-Al_2O_3 [10]. In those structures, ferric ions occupy four types of crystal positions: one undistorted octahedral (O1), two distorted octahedral (O2 and O3), and one distorted tetrahedral (T). At that, the sublattice magnetic moments are equal to: M (O1)=3.7 μ_B; M (O2)=−3.9 μ_B; M (O3)=3.9 μ_B, M (T)=−2.4 μ_B [11]. Thus the resulting net magnetic moment is due to the octahedral O1 sublattice, similar to ferrite spinel's.

As stated in Ref. [7], ε-Fe_2O_3 appears to be intermediate phase between γ-Fe_2O_3 and α-Fe_2O_3. Transformation of γ-Fe_2O_3 into ε-Fe_2O_3 or α-Fe_2O_3 depends on the degree of the virgin nanoparticles agglomeration. The matrix isolation or surface coatings can prevent them from agglomeration and thus stabilize the transient phase state. That is why the ε-Fe_2O_3 phase has never been observed in powdered samples. As concerns magnetic properties, Tronc and co-authors determined the ε-Fe_2O_3 nanoparticles synthesized [7] to belong to a non-collinear ferrimagnet though they did not exclude ε-Fe_2O_3 to be a four-sublattice collinear ferrimagnet. Similar results concerning crystal structure were

* Corresponding author.
E-mail address: ise@iph.krasn.ru (I.S. Edelman).

http://dx.doi.org/10.1016/j.jmmm.2015.10.126
0304-8853/

obtained by M. Gich with co-authors [12–14] synthesizing ε-Fe_2O_3 nanoparticles of ~25 nm [12, 13] or ~10 nm [14] in diameter with sol–gel chemistry followed by high-temperature treatments. (Parameters of orthorhombic cell $a=5.098(2)$, $b=8.785(3)$, and $c=9.468(2)$ Å that differs a little bit from those presented in [7]). A detailed study of the magnetization temperature behavior allowed these authors to establish that ε-Fe_2O_3 was a collinear ferrimagnet above 150 K, whereas the magnetic ordering below 80 K was characterized by a square-wave incommensurate structure. The transformation between these two states was a second-order phase transition and involved subtle structural changes mostly affecting the coordination of the tetrahedral and one of the octahedral Fe sites [12,13]. Besides, outstandingly high room-temperature coercivity (H_C~20 kOe) was revealed which drastically diminished upon cooling. J. Kohout with co-authors synthesized ε-Fe_2O_3 nanoparticles stabilized in an amorphous silica matrix by sol–gel technique [11]. Average nanoparticles diameter was ~25 nm; the lattice parameters of ε-Fe_2O_3 were $a=5.105(1)$ Å, $b=8.800(2)$ Å, $c=9.476(2)$ Å. Two-step magnetic phase transition spread between 100 K and 153 K was indicated; the first step in the temperature range of 153–130 K was related to the spin reorientation of the local magnetic moments in the magnetic sublattices and the second step at temperatures 130–100 K was supposed to be associated with the "intermediate spin" – "high spin" state transition of Fe^{3+} cations in the tetrahedral sublattice.

Another group of investigators presented recently rather small ε-Fe_2O_3 nanoparticles (beginning from 3.4 nm) which were prepared by impregnation of silica gel and aluminum oxide with $FeSO_4$ solutions [15–17]. It has been revealed that the state of iron depends on the nature of the support. Iron hydroxysulfate and iron oxysulfate nanoparticles were formed on the surface of silica gel, and iron oxide nanoparticles were formed on the surface of aluminum oxide. An increase in the concentration of iron ions or in the size of iron-containing particles led to hydration of the nanoparticle surface. The calcination of the samples resulted in the formation of ε-Fe_2O_3 oxide in a strongly disordered or amorphous state in iron-containing particles on the surface of silica gel. Two magnetic subsystems were revealed in the nanoparticles synthesized: paramagnetic subsystem was formed by the Fe^{3+} ions in the smallest (< 3.5 nm) particles' shell, while ferrimagnetic ordering in the "core" of the particles resulted in superparamagnetic behavior which was observed up to ~800 K. The magnetic moment of the particles was shown to be formed by both the ferrimagnetic ordering characteristic of ε-Fe_2O_3 core and an additional effect of uncompensated shell. The surface contribution, being of minor importance for the magnetic behavior of 25–100 nm particles, was shown to become essential when the particle size was below 10 nm.

The short review presented above showed the crucial role of the space confinement conditions in stabilizing of the metastable ε-Fe_2O_3 phase and adjusting its properties. In this connection, the development of other routes giving rise to ε-Fe_2O_3 nanoparticles is of interest.

Glasses doped with paramagnetic ions were the subject of numerous studies over a few last decades. At sufficiently high concentration of doping elements, magnetic nanoparticles appeared in the glass matrix, typically upon a deliberate thermal treatment (e.g., [18–26]). Some glass systems admitted magnetic nanoparticles precipitation even at low doping levels and thus preserved the optical transparency what allows to use magneto-optical methods for their investigation. Earlier, we have studied formation of ferrite nanoparticles in borate glasses co-doped with Fe and different transition ions both of 3d and 4f groups (e.g. [27–29]). Nanoparticles composition and structure have been shown to depend on glass matrix composition, nature and concentration of doping elements, and technological regimes. At that, magnetite, Fe_3O_4 [30], manganese ferrite [27], and maghemite, γ-Fe_2O_3 [28,29] nanoparticles were synthetized. Basing on the glass technology flexibility we aimed to synthesize ε-Fe_2O_3 nanoparticles in a glass matrix, investigate their properties in comparison with the nanoparticle properties in other matrices.

Here we present, for the first time, the emergence of ε-Fe_2O_3 nanoparticles in a borate glass matrix co-doped with Fe_2O_3 and Gd_2O_3. We focus upon the role of Gd_2O_3 concentration in nanoparticles formation and their properties.

2. Experimental details

2.1. Sample preparation

Glasses of the basic composition K_2O–Al_2O_3–B_2O_3 were synthesized using a technique described in Ref. [27]. Prior to the synthesis, 1.5 wt% Fe_2O_3 and Gd_2O_3 in different concentrations of 0.1, 0.2, 0.3, 0.4, 0.6, and 1.0 wt% (samples 1–6, correspondingly) with respect to basic glass composition were loaded in the charge. The mixtures were molten at 1100–1300 °C under oxidizing conditions. The melts were poured onto steel sheets, cooled down naturally to 380 °C. Then the glass plates were subjected to additional thermal treatment at the same conditions at 560 °C during 2 h.

2.2. Sample characterization

The XRD analysis was done at the "Structural Materials Science" beamline in the Kurchatov Synchrotron Radiation Centre (Moscow, Russia). The X-ray diffraction data were acquired in the transmission (Debye–Scherer) mode at a wavelength 0.696585 Å using a Fujifilm Imaging Plate as a 2D detector.

The visualization of particles formed in the glasses was carried out using electron microscope JEM-2200FS (JEOL Ltd.) operating in the high-resolution (HRTEM) and high-angle annular dark-field scanning (STEM-HAADF) transmission modes. Energy dispersive X-ray analysis (EDX) was used for the identification of chemical elements in the composition of glasses. Parameters of diffraction spots related to crystalline segregates were measured by fast Fourier transform (FFT) with the help of Digital Micrograph 3.3.1 (Gatan Ltd.) software. For the electron microscopic studies, the samples were finely ground, dispersed in ethanol, and deposited onto perforated carbon substrates attached to a standard copper grid and placed into the microscope UHV chamber.

Magnetic properties of the samples were studied with a superconducting quantum interference device (SQID) magnetometer at temperatures 78–300 K in the applied magnetic field up to 20 kOe.

Magneto-optical effects – magnetic circular dichroism (MCD) and Faraday effect (FE), were measured in energy interval 1.2–2.9 eV at temperatures 300 and 90 K. The external magnetic field and the light beam were directed normal to the sample plane. To obtain the high measurement's sensitivity, modulation of the light wave polarization state was used. The modulator was made of a fused silica prism with a glued piezoelectric ceramic element. When the ac voltage of frequency ω corresponding to the eigen-frequency of the system was supplied to the piezoelectric ceramics, an elastic stationary wave was excited in the quartz prism. Linearly polarized light with the polarization plane turned to an angle of 45° relatively the horizontal prism axis came on the prism. At the exit of the prism, the light polarization changes from the right- to the left-hand circle during one period of acoustic vibration of the prism. In the case of a sample possessing magneto-optical activity, its absorption coefficients and refractive indices are different for the right- and left-hand circular polarized light waves with respect to the magnetization direction of a sample. As a result, the intensity of the light having passed through the sample and, consequently, the

voltage at photomultiplier exit was modulated with the frequency ω when the MCD measuring and with 2 ω when FE measuring. Electromagnet with drilled poles provided the magnetic field up to 12 kOe. The MCD and FE values were measured as the difference between the photomultiplier voltages for two opposite directions of an applied magnetic field. The measurement accuracy was about 10^{-5}, and the spectral resolution was 20–50 cm^{-1} depending on the wavelength.

The electron spin resonance (ESR) spectra were recorded in the X band (9.46 GHz) with a Bruker EMX spectrometer equipped with an ER4112HV variable-temperature unit (300 and 120 K).

3. Results and discussions

3.1. Nanoparticles structural characteristics

X-ray diffraction patterns are shown in Fig. 1, a. They reveal several weak reflexes that are essentially the same for all samples studied. It seemed to be reasonable to compare the patterns with reference samples. The ε-Fe_2O_3 nanoparticles prepared by a wet chemical pore filling impregnation method with the iron (II) salt as a precursor were presented in [31]. With XRD, HRTEM, Mössbauer and electron resonance spectroscopy, authors of Ref. [31] proved that nanoparticles synthesized in such a way were the ε-Fe_2O_3 phase, indeed. We have chosen one type of these nanoparticles as a reference sample. Fig. 1, b shows XRD patterns for ε-Fe_2O_3 nanoparticles (curve 1) and for glass 1 (curve 2). Though a broad halo arising from the vitreous matrix hides partly the low-angle reflexes, the similarity of two curves is obvious, especially, in the region of 25-28 degrees. The average interplanar distances estimated from XRD patterns are listed in Table 1.

The STEM-HAADF images with different magnificent are shown in Fig. 2, a, b for the glass 1 and in Fig. 2, c, d for the glass 6 fragments. Nanoparticle segregates are seen as light spots of variable shapes. Both isolated particles (30-50 nm) and their conglomerates occur. HRTEM images showed that conglomerates consisted of small (2–8 nm) nanocrystals with different orientations; nanocrystals are located close to each other but separated by amorphous domains (Fig. 2, e and 3, a). Amorphous domains prevail in glasses with a higher Gd concentration (Fig. 3, a). This suggests that Gd atoms play an active role in the formation of ε-Fe_2O_3 nanoparticles.

Fig. 2, f and 3, b show several examples of the FFT for the glasses 1 and 6. Similar pictures were obtained for all samples. The set of crystallites interplanar spacing identified with FFT are listed in Table 1 (first column). It is difficult to identify the phase unambiguously because these values, taking in to account the measurement errors, can be assigned to several polymorph modifications of iron oxide. However comparison with data for ε-Fe_2O_3 nanoparticles obtained by several authors [2–5,7] shows that all interplanar spacing's for our glasses are close to those characteristic of this phase. The strongest coincidence is observed between the glass spacing's and the disordered ε-Fe_2O_3 spacing's. It should be noted that some distances coincide with distances for other iron oxide phases. For example, spacing's ~0.1981 nm and 0.1505 nm can be compared with 0.1940 and 0.1529 nm, corresponding to γ-Fe_2O_3 (PDF #39-1346); spacing's 0.2518 and 0.2501 nm can be compared with 0.2510 nm for α-Fe_2O_3 (PDF #19-0629) and also with 0.2530 nm for Fe_3O_4 (PDF #19-0629); spacing 0.1505 nm can be compare with 0.1540 nm for FeO (PDF #461312). However, no spacing's corresponding to the most intense lines of γ-Fe_2O_3 and α-Fe_2O_3 observed in the experimental pattern for our glass samples. Results of this comparison together with the XRD data (Fig. 1) allow making the quite reliable assignment of the crystal phase in the present glasses to be ε-Fe_2O_3, although the presence of other iron oxide phases cannot be excluded.

Let us turn now to the elements distribution in different regions of the glass samples. EDX analysis shows the adequacy of locally determined elemental concentrations of the glass matrix to

Table 1
Interplanar spacing's (nm) obtained with FFT and XRD (marked with *) for the studied glasses and X-ray diffraction data for ε-Fe_2O_3 presented in Refs. [2–5,7].

Glasses	Ref. [7]	Ref. [2]	Ref. [3]		Ref. [4]	Ref. [5]
			Ordered	Disordered		
0.2788*	0.2718	0.2728	0.274	–	0.280	0.279
0.2518	0.2541	0.2548	0.255	0.2529	0.254	0.253
0.2501	–	–	–	–	–	–
0.2284	0.2285	0.2295	–	–	–	–
0.2277	0.2237	0.2243	0.224	0.2229	0.224	0.223
0.2224	–	–	–		–	–
0.2032	0.2018	0.2018	–	–	–	–
0.1981	0.1992	0.1997	–	0.1971	–	–
0.175*	0.1732	0.1735	0.174	0.1725	0.173	0.173
0.1536*	0.1535	0.1537	0.154	–	–	–
0.1505	0.1518	0.152	0.152	0.1513	0.151	0.151
0.1490*	0.1469	0.1469	0.147	0.147	0.146	0.146

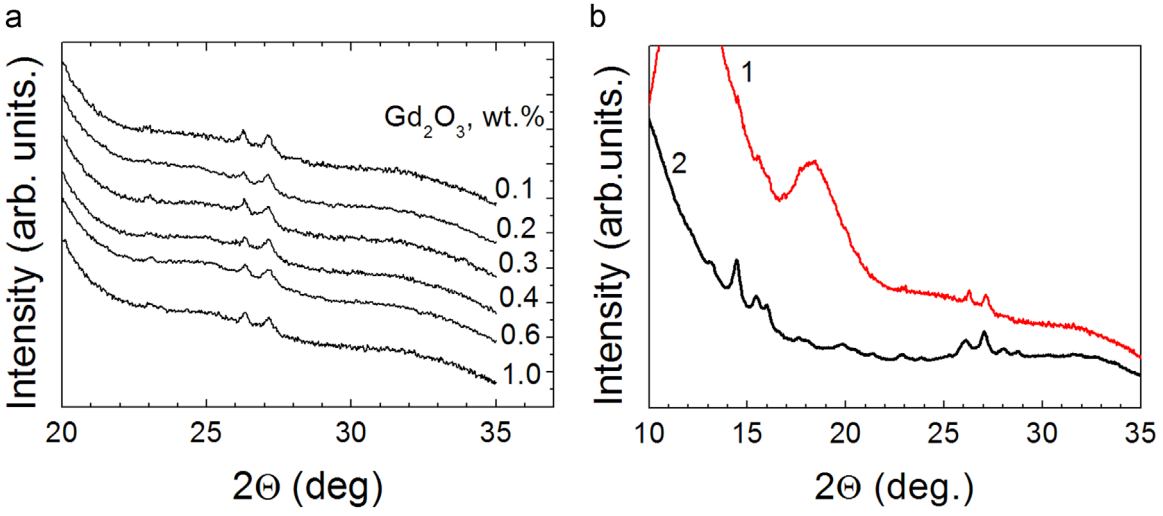

Fig. 1. X-ray diffraction patterns for all samples. Numbers to the right of the diffraction curves correspond to concentrations of Gd_2O_3 (a). Direct comparison of X-ray diffraction patterns for glass 1 (curve 1) and for ε-Fe_2O_3 nanoparticles (curve 2) (b).

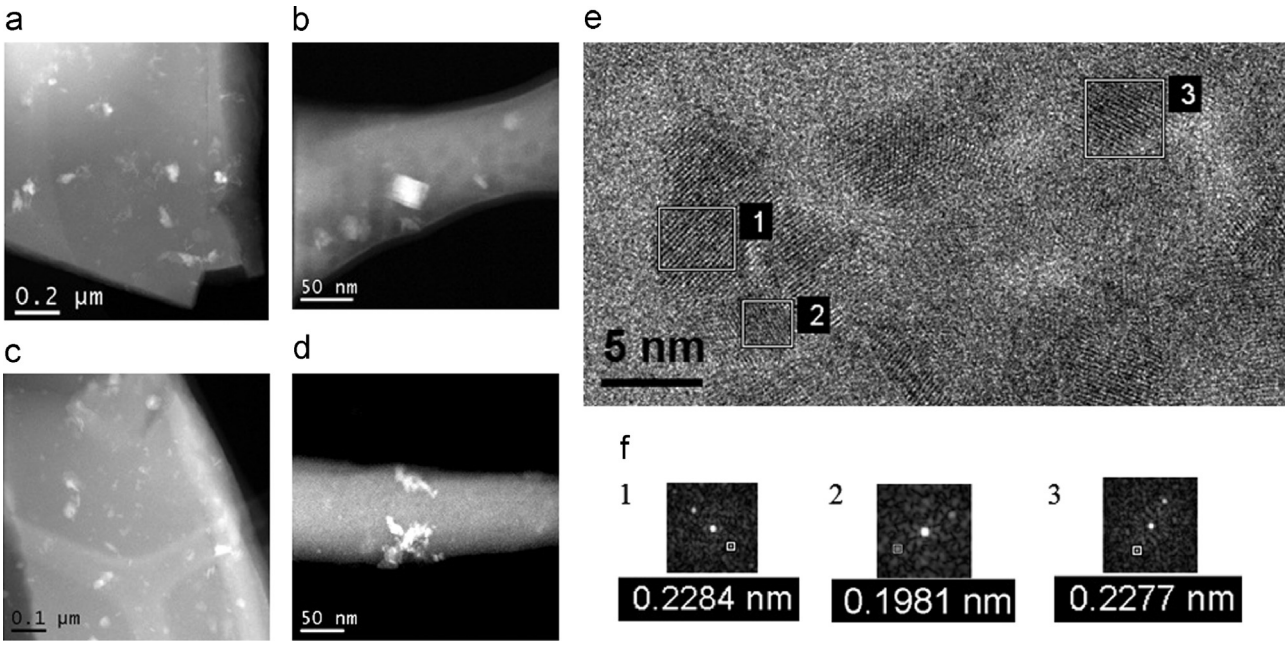

Fig. 2. STEM-HAADF images for samples 1 (a, b) and 6 (c, d); HRTEM image of the conglomerate region in glass 1 (e); FFT pictures with lattice constant for selected area 1, 2, 3 (f).

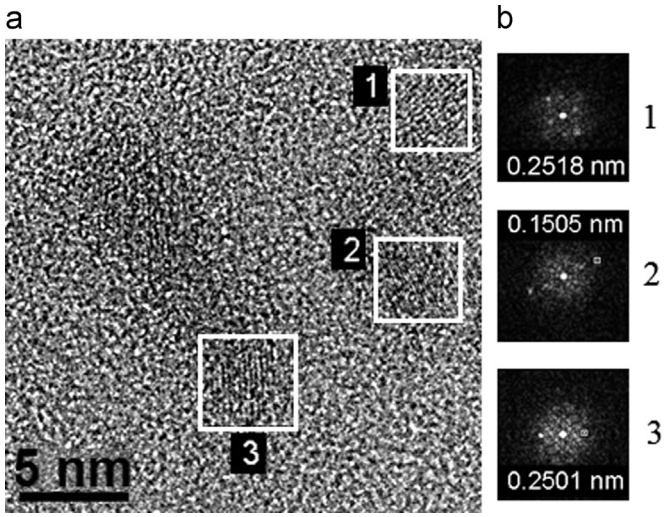

Fig. 3. HRTEM image of the conglomerate region in glass 6 (a); FFT pictures with lattice constant for selected area 1, 2, 3 (b).

the overall raw material composition used in the glass synthesis. Nevertheless, a totally different situation takes place when considering the elements' distribution inside the crystalline segregates. A small region of glass 6 is shown in STEM-HAADF image (Fig. 4, left). The EDX elemental mapping is shown in Fig. 4 demonstrating the Fe, Gd, and Al distribution in this region. Almost all Fe ions are seen to be localized inside the particle. Gd is also concentrated mostly inside the particles however it is also detected outside the particle, although in a lower concentration. At the same time, the basic glass-constituting elements are virtually absent in the region of the particle as it is demonstrated for Al in Fig. 4, right. Generally, analogues pictures are observed for all other samples.

Summarizing XRD and electron microscopy results, one can conclude the formation of ε-Fe_2O_3 nanoparticles. Other Fe oxides phases can be also presented as admixtures. Gd does not change the nanoparticle crystal structure although it is evidently incorporated into the iron oxide particles, probably as a disordered solid solution.

3.2. Magnetic properties

For all samples, the nonlinear magnetization vs. an external magnetic field with a hysteresis is observed. Typical curves are shown in Fig. 5 for samples with the minimal and maximal Gd contents. Magnetization increase with an increase of the magnetic field can be due to not only by the presence of magnetic nanoparticles but also by different paramagnetic centers. However the

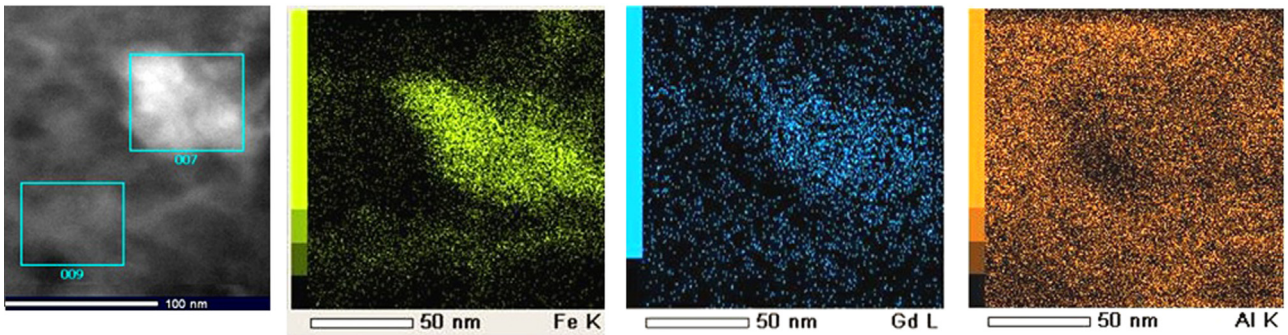

Fig. 4. STEM-HAADF image of the glass 6 small region (left). EDX elemental mapping: Fe (second from the left), Gd (third from the left), and Al (right). Atomic ratio Al: Fe: Gd is 35.6:58.8:5.6 for area «007» and 88.6:8.7:2.7 for area «009».

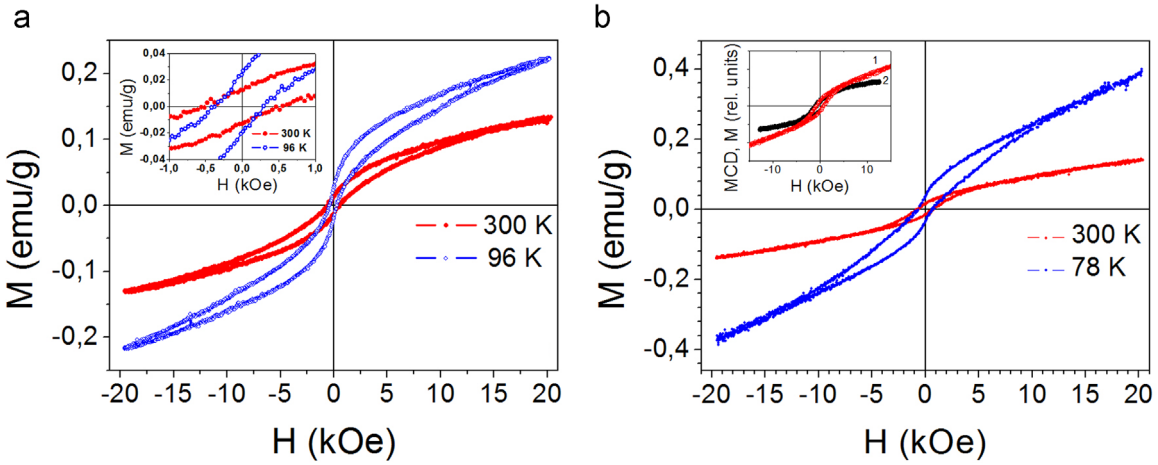

Fig. 5. Hysteresis loops obtained at two temperatures: left – for glass 1, insert: lower field region; right – for glass 6, insert: hysteresis loops recoded with SQID magnetometer (curve 1) and MCD at $E=2.5$ eV (curve 2) of glass 6 at room temperature.

hysteresis is uniquely associated with ferro- or ferri- magnetic particles. Insert in Fig. 5, b compares the magnetization vs. an external magnetic field of glass 6 obtained with MCD and with the SQID magnetometer. As MCD is especially sensitive to ferro- or ferri- magnetic components of the material under study, the difference between the two curves allows us to estimate the paramagnetic contribution into the apparent magnetization behavior. For glass 6, the paramagnetic contribution is about 20–30% of the total magnetization at room temperature in $H=12$ kOe. This contribution increases as temperature decreases as it seen from the slopes of the magnetization curves at two temperatures (Fig. 5, b). A similar magnetization behavior was observed for small ε-Fe_2O_3 nanoparticles in Ref. [15] and was associated with the surface defect-driven phenomena. As it is seen from the EDX elemental mapping (Fig. 4), in our case diluted paramagnetic ions present, which also contribute to the magnetization slope.

The branches of the room temperature hysteresis loops collapse at $H=12$ kOe for lower Gd concentration and at $H=5$ kOe for higher Gd concentration. Upon cooling, they do not collapse even at $H=20$ kOe for sample 1, while for sample 6 they collapse at $H=14$ kOe. For sample 1, the coercivity (H_C) is equal to 0.54 and 0.28 kOe at 300 and 96 K, respectively. Analogous values for sample 6 are 1.08 and 0.77 kOe at 300 and 78 K, respectively. So, we deal with a quite rare case when the hysteresis loop becomes narrower upon cooling. For comparison in the case of borate glasses containing γ-Fe_2O_3 nanoparticles, $H_C$increased from 0.05 kOe at room temperature to 0.15 kOe at 90 K – the behavior typical for superparamagnetic nanoparticles. A decrease of H_C upon cooling was observed by several authors for ε-Fe_2O_3 nanoparticles embedded into different matrices [12,13]. Thus, the H_C of the nanoparticles in a glass matrix in the present study is essentially lower as compared to pure ε-Fe_2O_3 nanoparticles [11,12,14] but the H_C vs. temperature behavior is similar to that of ε-Fe_2O_3 nanoparticles. Note, in the case of very small ε-Fe_2O_3 nanoparticles (4–5 nm) the H_C was about 5.5 kOe at 300 K [17] while for larger nanoparticles H_C was ~20 kOe [11,12,14].

3.3. Magnetic circular dichroism

The MCD spectra in the region of 2÷3 eV are presented in Fig. 6 for all samples at two temperatures. An intense broad maximum consisting, probably, of several overlapping components is observed in this region. Note that the MCD signal shape resembles the MCD spectrum observed earlier in Ref. [29] for the γ-Fe_2O_3 thin film and γ-Fe_2O_3 nanoparticles dispersed in a K_2O–Al_2O_3–B_2O_3–GeO glass (Fig. 7 curves 1 and 2, correspondingly). However the MCD value in the studied glasses is more than by a factor of 30 lower as compared to γ-Fe_2O_3 nanoparticles, though the Fe ions concentration in this case is only twice lower than in glass with γ-Fe_2O_3. In spite of the same Fe concentration in all samples, the MCD value changes noticeable from one sample to another. There is no clear correlation between the MCD intensity and the Gd_2O_3 concentration: the maximum MCD value at ~2.5 eV corresponds to 0.2 wt% of Gd_2O_3 at both temperatures;

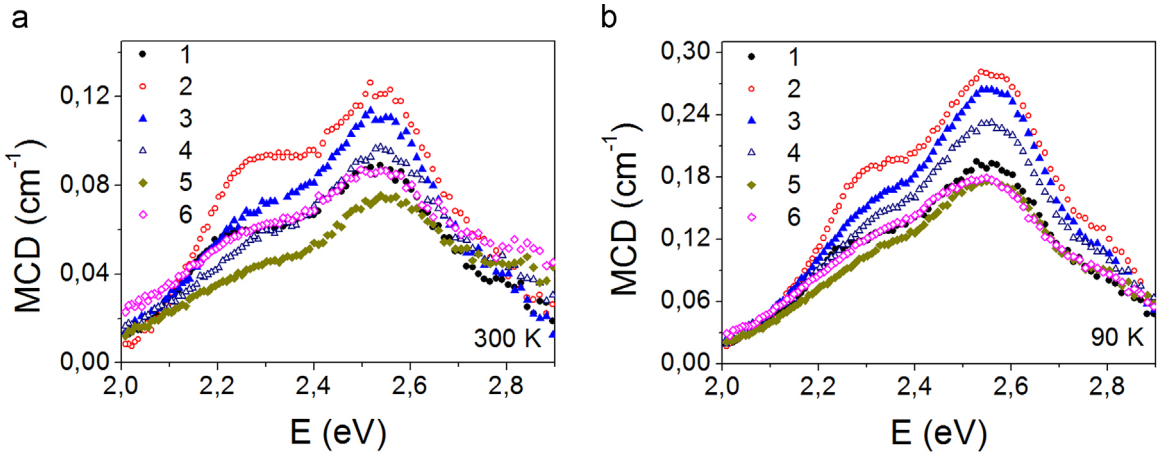

Fig. 6. MCD spectra at 300 K (left) and 90 K (right). The curve numbers correspond to the glass numbers. $H=3$ kOe.

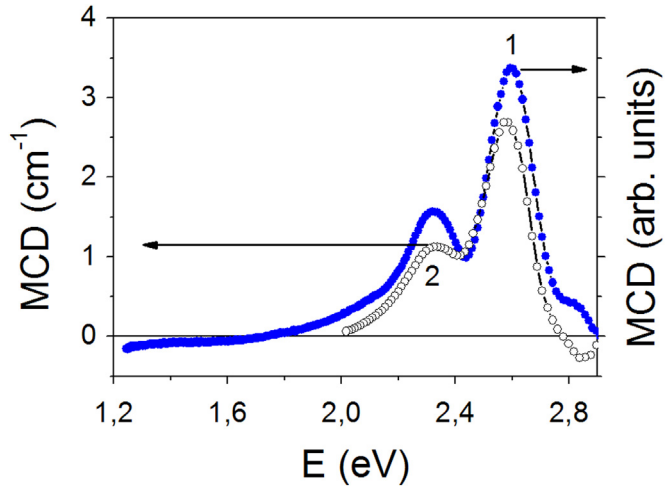

Fig. 7. MCD for γ-Fe_2O_3 thin film (curve 1, right axis) and γ-Fe_2O_3 nanoparticles dispersed in a glass matrix (curve 2, left axis).

the minimum MCD value at this energy is observed at 300 K for 0.6 wt% of Gd_2O_3, however at 90 K the equal MCD values are observed for 0.6 and 1.0 wt% of Gd_2O_3. Another remarkable feature is a strong MCD increase (more than by a factor of 2) upon cooling from 300 to 90 K. Such a strong temperature jump of the magneto-optical value has been observed neither for other glass-based

Table 2
Parameters of the Gaussian components best fitted to the experimental MCD curves at two temperatures for two glass samples with lower and higher Gd concentrations as well as for γ-Fe_2O_3 thin film: peak position (*E*, eV), amplitude (A, cm^{-1}) and HWHM (Δ*E*, eV).

Glass 1						
Peak	*T*=300 K			*T*=90 K		
	E, eV	*A*, cm^{-1}	Δ*E*, eV	*E*, eV	*A*, cm^{-1}	Δ*E*, eV
*E*2	2.23	0.053	0.1344	2.2724	0.104	0.138
*E*3	2.54	0.088	0.1606	2.2585	0.186	0.146
Glass 6						
Peak	*T*=300 K			*T*=90 K		
	E, eV	*A*, cm^{-1}	Δ*E*, eV	*E*, eV	*A*, cm^{-1}	Δ*E*, eV
*E*2	2.23	0.045	0.130	2.26	0.080	0.133
*E*3	2.53	0.084	0.170	2.54	0.175	0.167
γ-Fe_2O_3 film						
Peak	*T*=300 K			*T*=90 K		
	E, eV	A, rel. un.	Δ*E*, eV	Energy, eV	*A*, rel. un.	Δ*E*, eV
*E*2	2.33	0.421	0.096	2.35	0.508	0.091
*E*3	2.59	1.0	0.917	2.61	1.305	0.086

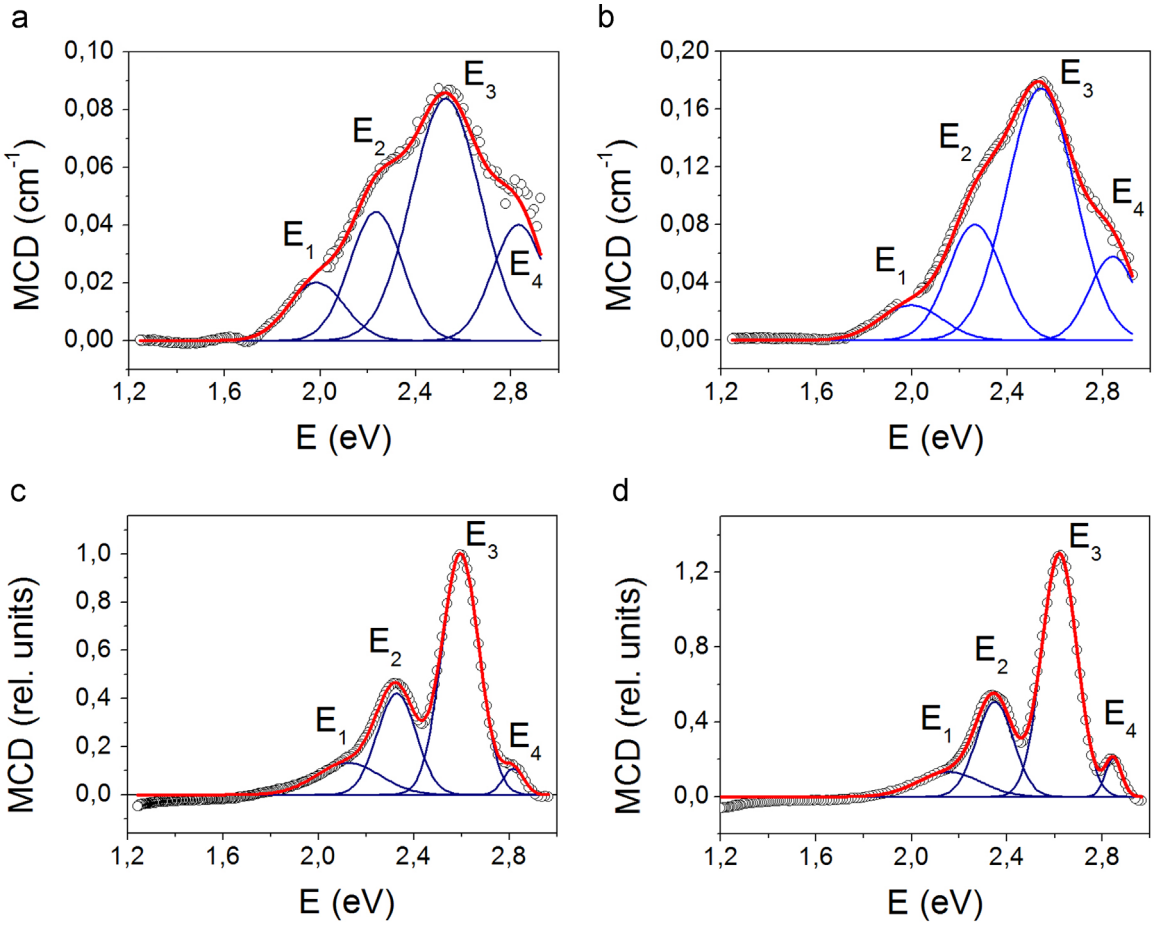

Fig. 8. MCD spectrum decomposition to individual components of the Gaussian shape *E*1, *E*2, *E*3, *E*4 at *T*=300 K (a, c) and *T*=90 K (b, d) for sample 6 (a, b) and γ-Fe_2O_3 thin film (c, d). Bold red lines are the sums of four components, circles are the experimental data. (For interpretation of the references to color in this figure legend, the reader is referred to the web version of this article.)

systems with ferrite-spinel nanoparticles dispersed (e. g., γ-Fe_2O_3 [29]) no for ferrite spinel thin films [32]).

To analyze the MCD spectra in more details and make adequate comparison between the samples, we decomposed the MCD spectra into several Gaussian components. We supposed all the maxima to be of the paramagnetic line shape. The examples of the decomposition are shown in Fig. 8 (a, b) for glass 6 at two temperatures. The best fit to the experimental curves has been obtained with four lines with parameters presented in Table 2. Further, we shall analyze two central lines *E*2 and *E*3 as their parameters are determined most reliably as compared to outer lines *E*1 and *E*4 which can be distorted by MCD maxima outside the spectral range investigated. For the sake of comparison, similar decomposition of the MCD spectra of γ-Fe_2O_3 thin film (prepared with self-propagating high-temperature synthesis) is shown also (Fig. 8 (c, d)). The MCD maximum energies and the ratio of the main maxima, *E*2 and *E*3, amplitudes are close for all samples (Table 2). In the case of thin film, *E*2 and *E*3 maxima shift insignificantly to higher energies. The amplitudes ratio $E3/E2 \sim 1.8$ for glass and 2.4 for thin film. Upon cooling the *E*2 and *E*3 amplitudes increase is about 1.85 and 2.1, correspondingly, for glasses, and about 1.2 and 1.3 for thin film. The maximum widths ΔE for the glass samples are noticeably higher in comparison with γ-Fe_2O_3 thin film. The ratio of the maximum amplitudes and their temperature changes together with very small MCD value comparing to glasses with γ-Fe_2O_3 (compare Fig. 6(a) and curve 2 in Fig. 7) allow supposing the nanoparticles nature in the investigated glasses to be different from γ-Fe_2O_3. Other Fe oxides, Fe_3O_4 and α-Fe_2O_3 also can be excluded from the consideration. Fe_3O_4 is characterized by quite different MCD spectral dependence [28,33]. Hematite α-Fe_2O_3 is characterized by the Morin transition at ~250 K at that the total magnetic moment disappears. There is no such an effect in our case. Taking into account that Gd is present in the glass composition one could speculate the nanoparticles composition to be close to the gadolinium-iron-garnet. To check for this suggestion, we compare the FE spectra of garnet and our glasses, taking into account that the resulting magnetic moment of garnet-ferrite is due to tetrahedral coordinated Fe^{3+} ions while the ε-Fe_2O_3 net moment is primarily associated with the octahedral coordinated Fe^{3+} ions. That is why FE should be of different signs in these two cases, as it was shown for $Y_3Fe_5O_{12}$ and for γ-Fe_2O_3 with the net magnetic moment determined by the octahedral Fe^{3+} sublattice [33].

In the spectral region investigated the FE spectra of all rare earth garnets have identical shapes similar to that of yttrium-iron-garnet and are characterized by the positive sign [34]. Room temperature FE spectra of glass 1 and of $Y_3Fe_5O_{12}$ thin film are compared in Fig. 9. Opposite FE signs and spectral shapes in these two cases allow us to decisively exclude the garnet nanoparticles formation in glasses. Thus the complex analysis of XRD, HRTEM, magnetic and MCD measurements support the formation of ε-Fe_2O_3 nanoparticles in the glasses under investigation.

There is nothing strange in the coincidence of the MCD spectrum shapes for γ-Fe_2O_3 and ε-Fe_2O_3 nanoparticles. Both these compounds contain Fe^{3+} ions in similar crystal positions: octahedral and tetrahedral. That is why the structure of the energy levels and a set of electron transitions are the same in both cases. The crystal structure distortions, defects and disorder in ε-Fe_2O_3 should affect the line widths. Indeed, for the present glass samples the MCD lines are wider compared to γ-Fe_2O_3 films (Table 2). Analogously to γ-Fe_2O_3, we can refer *E*2 and *E*3 maxima to electron transitions to the excited states $^6A_1(^6S)$-$^4A_1$, $^4E(^4G)$ in tetrahedral (*E*3) and octahedral (*E*2) positions.

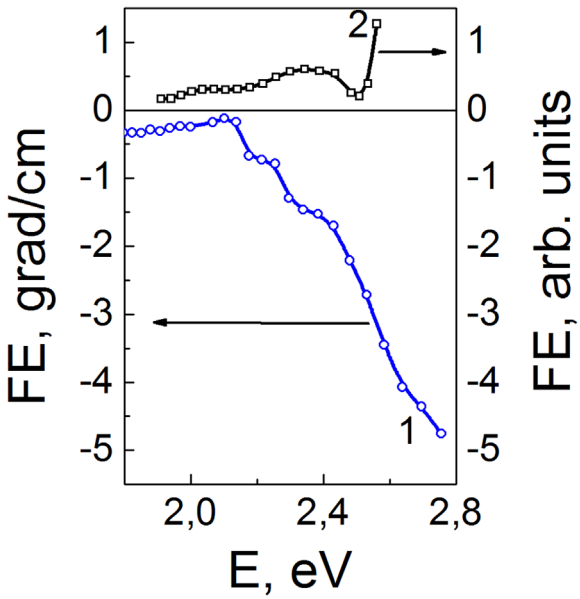

Fig. 9. FE spectra for glass 1 (curve 1) and $Y_3Fe_5O_{12}$ film (curve 2) at room temperature.

3.4. Electron magnetic resonance

EMR spectra recorded at 300 and 120 K for glasses 1 and 6 are shown in Fig. 10. The shape of the spectra is close to that observed in [16,35] for ε-Fe_2O_3 nanoparticles deposited on silica gel. Two main resonance lines dominate the EMR spectra: one with $g \sim 4.25$ whose intensity increases as temperature decreases and other one with $g \sim 2$ whose intensity decreases with temperature. Ratio of the low-field and high-field line intensities changes from one sample to another as a function of Gd concentration. The first line is associated with the diluted paramagnetic ions, the g-factor value is characteristic for paramagnetic ions occupying tetrahedral positions in a glass. Both Fe^{3+} and Gd^{3+} ions can play role of such centers as it follows from the comparison of the lower field line intensities for samples with minimum and maximum Gd content taking into account the same Fe concentrations in all samples. Insert to Fig. 10 (right) shows enlarged low-field region obtained with subtracting the Fe^{3+} line in the glass containing only Fe from the line in the glass 6 spectrum. The obtained line is very close in shape to the low-field line presented in Ref. [36] for borate glasses containing diluted Gd ions. This line is seen to be of the other shape, namely, the signal is of the opposite sign relatively to the total signal. That is why the Gd contribution decreases the total signal. In reality, the total signal intensity increases with Gd concentration in a glass (compare Fig. 10 a and b). This fact is associated with an increase in the concentration of paramagnetic diluted Fe ions and, vice-versa, a decrease in the concentration of Fe ions in nanoparticles.

Consider now the main line (high field) of the EMR spectrum. This line intensity decreases with temperature that is characteristic of superparamagnetic particles. The same behavior was observed in [36] for EMR line with $g \sim 2$ of silica-supported ε-Fe_2O_3 nanoparticles with the average size of a few nanometers. For all samples this line is rather broad and non-symmetric, reflecting the magnetic inhomogeneity of nanoparticles, and it cannot be presented by a single Lorentzian. To interpret the whole EMR spectra, we decomposed them to a minimal sufficient set of the Lorentz lines. The best fit with experimental spectra was obtained using five lines. An example of the decompositions is shown in Fig. 11 for sample 1. Line L5 refers to the low-field line discussed above. The high-field part of the spectrum is presented by two narrow lines

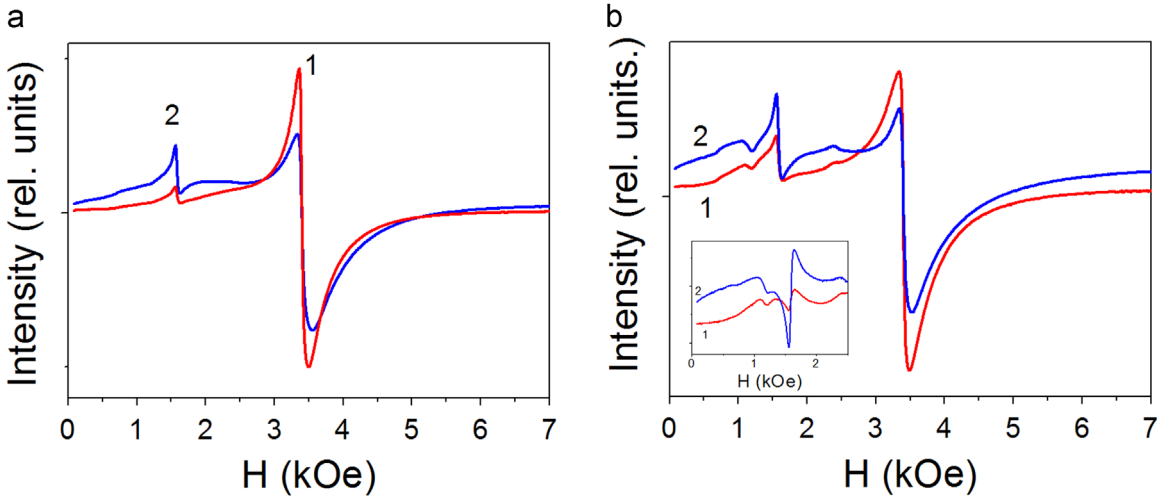

Fig. 10. EMR spectra for glasses 1 (a) and 6 (b) at 300 K (curves 1, red) and 120 K (curves 2, blue). Insert: low-field region EMR spectrum of the glass 6 after subtracting of the spectrum of the glass containing no Gd. (For interpretation of the references to color in this figure legend, the reader is referred to the web version of this article.)

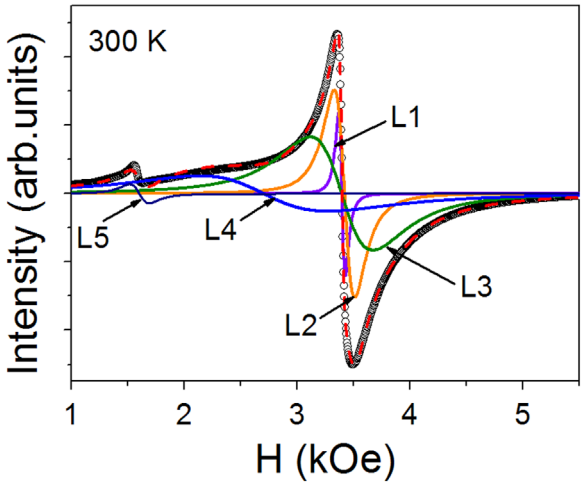

Fig. 11. EMR spectrum decomposition to individual components of the Lorentz shape L1, L2, L3, L4, L5 for glass 1 at T=300 K.

L1 and L2 and two very wide lines L3 and L4. Parameters of the L1–L4 lines are summarized in Table 3. It is seen that two pairs of lines differ strongly from each other. For all samples, g-factor of L1 and L2 lines is very close to 2, that is characteristic of Fe^{3+} ions in the octahedral surroundings. The fact that $g<2$ can evidence ferromagnetic interactions inside the particles [37, p. 144]. The small widths of L1 and L2 lines indicate a narrow distribution of nanoparticle sizes [38]. Indeed, almost ideal nano-crystallites of close dimensions are seen in Fig. 2, c. The L2 line width is larger compared to that of L1. This makes it possible to attribute L1 to undistorted octahedrons and L2 – to distorted ones. In both cases the line width increases with an increase in the Gd concentration. If it is correct, the incorporation of Gd into iron oxide nanoparticles should increase distortions and thus give rise to an increase in the crystal anisotropy. As Fe concentration inside the particles decreases in this case, the quantity of diluted Fe ions will increase as well as the EMR signal (g=4.3) associated with them that is observed in reality.

Line L3 is characterized by $g\approx 2$ at 300 K and demonstrates a significant g increase at 120 K. Besides, this line is rather wide and its width increases as temperature decreases. The line intensity decreases with Gd concentration increase similar to the L1 and L2 lines. Such a behavior can imply the line L3 to be associated with the nanoparticles' surface region. As it was shown in many studies,

Table 3
Parameters of the components of the EMR spectra at 300 and 120 K for all glass samples 1–6.

Line L1	g-factor		dH, Oe		I*10^6, rel. un.	
	300 K	120 K	300 K	120 K	300 K	120 K
1	1.993	1.991	48.7	88.9	0.482	0.37
2	1.994	1.991	53.1	110.6	0.47	0.25
3	1.993	1.989	56.2	127.8	0.35	0.27
4	1.993	1.993	53.8	89.6	0.42	0.24
5	1.993	1.987	61.0	145.6	0.23	0.22
6	1.990	1.986	77.0	119.7	0.23	0.19
Line L2						
1	1.980	1.973	157.7	336.0	0.61	0.45
2	1.982	1.976	163.8	384.6	0.60	0.33
3	1.982	1.977	172	469.8	0.51	0.30
4	1.982	1.972	164.3	286.6	0.64	0.35
5	1.982	1.986	188.5	546.7	0.23	0.22
6	1.987	1.989	311.7	552.6	0.23	0.15
Line L3						
1	1.996	2.211	480.6	1088.7	0.33	0.22
2	1.909	2.278	510.0	1201.4	0.35	0.23
3	1.997	2.415	527.6	1161.6	0.28	0.16
4	1.996	2.060	498.4	836.6	0.40	0.26
5	1.995	2.568	558.4	1233	0.19	0.12
6	2.206	2.442	1019.7	700.7	0.08	0.05
Line L4						
1	2.507	3.420	981.6	988.0	0.10	0.10
2	2.532	3.563	964	883.8	0.09	0.08
3	2.543	3.740	911	778.8	0.11	0.06
4	2.471	2.906	1359	1297	0.10	0.14
5	2.584	3.989	1069	392	0.06	0.03
6	3.684	3.441	763.3	1532	0.04	0.05

in particularly in Ref. [39], the surface anisotropy makes an essential contribution in the nanoparticles magnetic anisotropy and it can be rather large. On the other hand, the strong g-factor increase at temperature decrease can indicate the spin glass behavior of the particles surface: at higher temperatures there is spin disorder in the surface and at lower temperatures the surface spins order antiferromagnetic [40]. The low intensity L4 line differs strongly from other lines; there is no regularity in the dependence of its width and intensity on Gd concentration. Its origin is currently unclear. Supposition is possible this line to be associated with very thin glass layers separating the particles in conglomerates (Fig. 2, d).

Summarizing results of the structural, static magnetic, magneto-optical and EMR studies, one can make a statement on the

emergence of ε-Fe_2O_3 nanoparticles in Al_2O_3–K_2O-B_2O_3 glasses co-doped with low concentrations of Fe (1.5 wt%) and Gd (0.1–1.0 wt%). To our best knowledge, the possibility of this Fe oxide phase to be formed in a glass matrix has not been reported so far. Quite contrary it was shown earlier that only Fe_3O_4 or α-Fe_2O_3 nanoparticles arise in glasses of analogous basic compositions doped with Fe_2O_3 only in dependence on the Al_2O_3/K_2O ratio [41]. When GeO_2 is introduced in the basic glass composition and rare earth oxides are used as doping elements together with Fe_2O_3, γ-Fe_2O_3 nanoparticles are typically formed [29]. Thus, we believe that it is the basic glass composition and Gd doping that provides appropriate conditions for the ε-Fe_2O_3 nanoparticles formation. Besides, the dependence of the glass properties on Gd concentration, as well as the EDX elemental mapping (Fig. 4) clearly indicates the incorporation of Gd into the iron oxide particles. We speculate that Gd can substitute Fe atoms in crystal positions and can form extra phases at the intergrain boundaries inside the particles or in the near-surface regions. In our case all three possibilities can be realized. To elucidate this question, additional investigations are necessary that are currently underway.

4. Conclusions

Nanocrystalline magnetic particles are shown to form in (K_2O–Al_2O_3–B_2O_3) glasses co-doped with Fe_2O_3 (1.5 wt%) and Gd_2O_3 in concentrations ranging from 0.1 to 1.0 wt% above 100% of the basic glass composition. According to XRD, STEM-HAADF, EDX data, static magnetic measurements, MCD and EMR results, nanoparticles are assigned to the ε-Fe_2O_3 iron oxide phase. The doping elements distribution in different areas of the glasses was obtained: virtually all Fe and the dominant fraction of Gd ions are concentrated inside the particles. The set of interplanar spacing's obtained from XRD and SAED closely resembles ε-Fe_2O_3. Magneto-optical effects for this compound are investigated here for the first time. The MCD spectrum characteristics depend non-monotonically on Gd concentration. An analysis of MCD and EMR data has shown that it is Gd that regulates the process of nanoparticles formation by partial incorporation into them that is manifested in changes of MCD value and EMR spectrum characteristics.

Acknowledgments

This work was supported partly by the Russian Foundation for Basic Research, Grants No 14-02-01211-a and by the President of Russia Grant No. NSh-2886.2014.2. Authors are grateful to G.A. Bukhtiyarova and O.N. Martyanov for the assistance in the ε-Fe_2O_3 nanoparticles prepared by a wet chemical pore filling impregnation method and for the discussion of the obtained results.

References

[1] H. Forestier, G. Guiot-Guillain, New ferromagnetic variety of ferric oxide, C. R. Acad. Sci. 199 (1934) 720.
[2] R. Schrader, G. Buttner, Eine neue Eisen(III)-oxidphase: e-Fe_2O_3, *Z.*, Anorg. Allg. Chem. 320 (1963) 220–234.
[3] L. Walter-Levy, E. Quemeneur, On the hydrolysis of ferric sulphate at 100 °C, C. R. Acad. Sci. 257 (1963) 3410.
[4] J.M. Trautmann, H. Forestier, Preparation and study of ε-Fe_2O_3, C. R. Acad. Sci. 261 (1965) 4423.
[5] I. Dezsi, J.M.D. Coey, Magnetic and thermal properties of e-Fe_2O_3, Phys. Status Solidi A 15 (1973) 681–685.
[6] Powder Diffraction File No. 16-653, JCPDS-International Center for Diffraction Data, Swarthmore, PA, 1993.
[7] E. Tronc, C. Chaneac, J.P. Jolivet, Structural and magnetic characterization of e-Fe_2O_3, J. Solid State Chem. 139 (1998) 93–104.
[8] S.C. Abrahams, J.M. Reddy, J.L. Bernstein, Crystal structure of piezoelectric ferromagnetic gallium iron oxide, J. Chem. Phys. 42 (1965) 3957–3968.
[9] F. Bouree, J.L. Badour, E. Elabraoui, J. Musso, C. Laurent, A. Rousset, Crystal and magnetic structure of piezoelectric, ferrimagnetic and magnetoelectric aluminium iron oxide $FeAlO_3$ from neutron powder diffraction, Acta Crystallogr. Sect. B 52 (1996) 217–222.
[10] L. Smreok, V. Langer, M. Halvarsson, S.Z. Ruppi, A new Rietveld refinement of k-Al_2O_3, Z. Kristallogr. 216 (2001) 409–412.
[11] J. Kohout, P. Brazda, K. Zaveta, D. Kubaniova, T. Kmjec, L. Kubıckova, M. Klementova, E. Santava, A. Lancok, The magnetic transition in e-Fe_2O_3 nanoparticles: magnetic properties and hyperfine interactions from Mossbauer spectroscopy, J. Appl. Phys. 117 (2015) 17D505.
[12] M. Gich, A. Roig, C. Frontera, E. Molins, J. Sort, M. Popovici, G. Chouteau, D. M. Marero, J. Nogues, Large coercivity and low-temperature magnetic reorientation in ε-Fe_2O_3 nanoparticles, J. Appl. Phys. 98 (2005) 044307.
[13] M. Gich, C. Frontera, A. Roig, E. Taboada, E. Molins, H.R. Rechenberg, J.D. Ardisson, W. A.A. Macedo, C. Ritter, V. Hardy, J. Sort, V. Skumryev, J. Nogues, High- and low-temperature crystal and magnetic structures of ε-Fe_2O_3 and their correlation to its magnetic properties, Chem. Mater. 18 (2006) 3889–3897.
[14] M. Popovici, M. Gich, D. Niznansky, A. Roig, C. Savii, L. Casas, E. Molins, K. Zaveta, C. Enache, J. Sort, S. de Brion, G. Chouteau, J. Nogues, Optimized synthesis of the elusive ε-Fe_2O_3 phase via sol–gel chemistry, Chem. Mater. 16 (2004) 5542–5548.
[15] D.A. Balaev, A.A. Dubrovskiy, K.A. Shaykhutdinov, O.A. Bayukov, S.S. Yakushkin, G. A. Bukhtiyarova, O.N. Martyanov, Surface effects and magnetic ordering in few-nanometer-sized e-Fe_2O_3 particles, J. Appl. Phys. 114 (2013) 163911.
[16] S.S. Yakushkin, G.A. Bukhtiyarova, O.N. Martyanov, Formation conditions of a magnetically ordered phase ε-Fe_2O_3. A FMR in situ study, J. Struct. Chem. 54 (2013) 876–882.
[17] D.A. Balaev, I.S. Poperechny, A.A. Krasikov, K.A. Shaikhutdinov, A.A. Dubrovskiy, S. I. Popkov, A.D. Balaev, S.S. Yakushkin, G.A. Bukhtiyarova, O.N. Martyanov, Yu. L. Raikher, Dynamic magnetization of ε-Fe_2O_3 in pulse field: evidence of surface effect, J. Appl. Phys. 117 (2015) 063908.
[18] A. Hoell, A. Wiedenmann, U. Lembke, R. Kranold, The non-magnetic surface of magnetic particles in nanostructured glass ceramics studied by SANS, Physica B 276 (2000) 886–887.
[19] A. Karamanov, R. Di Gioacchino, P. Pisciella, M. Pelino, Glass transformation range of iron rich glass and glass ceramics determined by different methods, Glass Technol. 42 (2001) 126–129.
[20] S. Woltz, R. Hiergeist, P. Gornert, C. Rüssel, Magnetite nanoparticles prepared by the glass crystallization method and their physical properties, JMMM 298 (2006) 7–13.
[21] H. Akamatsu, K. Tanaka, K. Fujita, S. Murai, Magnetic phase transitions in $Fe_2O_3-Bi_2O_3-B_2O_3$ glasses, J. Phys.: Condens. Matter 20 (2008) 235216.
[22] K. Sharma, Sh Singh, C.L. Prajapat, S. Bhattacharya, M.R. Jagannath, S.M. Singh, Yusuf, G.P. Kothiyal, Preparation and study of magnetic properties of silico phosphate glass and glass-ceramics having iron and zinc oxide, JMMM 321 (2009) 3821–3828.
[23] R. Harizanova, I. Gugov, C. Russel, D. Tatchev, V.S. Raghuwanshi, A. Hoell, Synthesis and characterization of nano-sized ferrimagnetic particles with potential applications in medicine and sensor technology, J. Mater. Sci. 46 (2011) 7169–7176.
[24] P. Pascuta, A. Vladescu, G. Borodi, E. Culea, R. Telean, Synthesis, structural and magnetic characterization of iron-zinc-borate glass ceramics containing nanocrystalline zinc ferrite, J. Mater. Sci. Mater. Electron. 23 (2) (2012) 582–588.
[25] V.S. Raghuwanshi, R. Harizanova, D. Tatchev, A. Hoell, C. Russel, Structural analysis of Fe–Mn–O nanoparticles in glass ceramics by small angle scattering, J. Solid State Chem. 222 (2015) 103–110.
[26] S.N. Garaje, S.K. Apte, G. Kumar, R.P. Rajendra, S.D. Naik, S.M. Mahajan, R. Chand, bB. Kale, Ferric oxide quantum dots in stable phosphate glass system and their magneto-optical study, Mater. Res. Bull. 48 (2) (2013) 901–906.
[27] J. Kliava, I. Edelman, O. Ivanova, R. Ivantsov, E. Petrakovskaja, L. Hennet, D. Thiaudiere, M.-L. Saboungi, Electron magnetic resonance and magnetooptical studies of nanoparticle-containing borate glasses, JMMM 323 (2011) 451–460.
[28] I. Edelman, O. Ivanova, R. Ivantsov, D. Velikanov, V. Zabluda, Y. Zubavichus, A. Veligzhanin, V. Zaikovskiy, S. Stepanov, A. Artemenko, J. Curély, J. Kliava, Magnetic nanoparticles formed in glasses co-doped with iron and larger radius elements, J. Appl. Phys. 112 (2012) 084331.
[29] I.S. Edelman, O.S. Ivanova, E.A. Petrakovskaja, D.A. Velikanov, I.A. Tarasov, Y. V. Zubavichus, N.N. Trofimova, V.I. Zaikovskii, Formation, characterization and magnetic properties of maghemite γ-Fe_2O_3 nanoparticles in borate glasses, J. Alloy. Compd. 624 (2015) 60–67.
[30] G.T. Petrovsky, I.S. Edelman, C.A. Stepanov, T.V. Zarubina, T.A. Kim, Magneto-optical properties of alumino-borate glasses doped with the transition metal oxides, Glass Phys. Chem. Glass Phys. Chem. 20 (6) (1994) 748–763.
[31] G.A. Bukhtiyarova, M.A. Shuvaeva, O.A. Bayukov, S.S. Yakushkin, O.N. Martyanov, Facile synthesis of nanosized e-Fe_2O_3 particles on the silica support, J. Nanopart. Res. 13 (2011) 5527–5534.
[32] G.A. Gehring, M.S. Alshammari, D.S. Score, J.R. Neal, A. Mokhtari, A.M. Fox, Magneto-optic studies of magnetic oxides, JMMM 324 (2012) 3422–3426.
[33] H. Wang, J. Shen, Magneto-optic faraday rotation of sputtered γ-Fe_2O_3 film, JMMM 73 (1988) 103–105.
[34] P. Hansen, J.P. Krume, Magnetic and magneto-optical properties of garnet films, Thin solid Films 114 (1984) 69–107.
[35] S.S. Yakushkin, A.A. Dubrovskiy, D.A. Balaev, K.A. Shaykhutdinov, G.A. Bukhtiyarova, O.N. Martyanov, Magnetic properties of few nanometers e-Fe_2O_3 nanoparticles supported on the silica, J. Appl. Phys. 111 (2012) 044312.
[36] J. Kliava, A. Malakhovskii, I. Edelman, A. Potseluyko, E. Petrakovskaja, S. Melnikova, T. Zarubina, G. Petrovskii, Y. Bruckental, Y. Yeshurun, Unusual magnetic transitions and nature of magnetic resonance spectra in oxide glasses containing gadolinium, Phys. Rev. B 71 (2005) 104406.
[37] S.A. Altshuler, B.M. Kozirev, Electron Paramagnetic Resonance of the Compositions of Gapy Group Elements, Nauka Press, Moscow (1972), p. 670.
[38] R.S. Beasi, T.C. Devezas, Anisotropy field of small magnetic particles as measured by resonance, J. Appl. Phys. 49 (4) (1978) 2466.
[39] S.P. Gubin, Yu. A. Koksharov, G.B. Khomutov, G. Yurkov, Magnetic nanoparticles:

preparation, structure and properties, Russ. Chem. Rev. 74 (6) (2005) 489–520.
[40] R.H. Kodama, A.E. Bertkowitz, E.J. McNiff, S. Foner, Surface spin disorder in ferrite nanoparticles (invites), J. Appl. Phys. 81 (8) (1997) 5552–5557.
[41] S.A. Stepanov, I.S. Edelman, T.A. Kim, G.T. Petrovsky, G.V. Popov, Properties of magnetically ordered microparticles in borate glasses, Phys. Stat. Sol. A 104 (1987) 805–813.